INL/RPT-24-80710

Light Water Reactor Sustainability Program

Development of New Reactor Core Configuration for Power Uprate – Fuel Reload & Heat Processing Analyses, Core Design, System Safety Assessments, and Fuel Performance Analyses

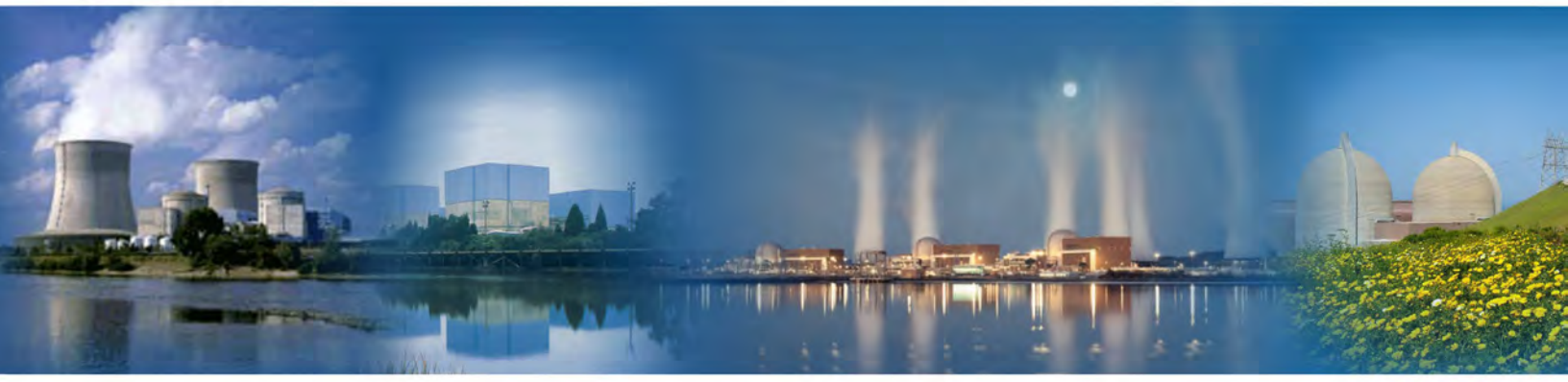

September 2024

U.S. Department of Energy

Office of Nuclear Energy

INL/RPT-24-80710

Development of New Reactor Core Configuration for Power Uprate – Fuel Reload and Heat Processing Analyses, Core Design, System Safety Assessments, and Fuel Performance Analyses

Svetlana Lawrence[1]
Carlo Parisi[1]
Robby Christian[1]
Junyung Kim[1]
Courtney Otani[1]
Juan Cristhian Luque Gutierrez[2]
Nicholas Rollins[2]
Jason Hou[2]

[1] Idaho National Laboratory
[2] North Carolina State University

September 2024

Prepared for the
U.S. Department of Energy
Office of Nuclear Energy
Under DOE Idaho Operations Office
Contract DE-AC07-05ID14517

Page intentionally left blank

EXECUTIVE SUMMARY

With the passage of the Infrastructure Investment and Jobs Act in 2021 and the Inflation Reduction Act in 2022, the United States stands at a critical juncture for the future of nuclear power. These landmark policies provide significant support for clean energy initiatives, positioning nuclear power as a key component of the nation's strategy to reduce carbon emissions and achieve energy security. This growing emphasis on nuclear energy is driven by the need for reliable, low-carbon power sources as the country transitions away from fossil fuels. Federal policy, along with increasing state-level support, is encouraging investment in nuclear technology advancements to meet these demands.

Building new nuclear power plants (NPPs), however, presents significant challenges due to high costs and long construction timelines. As a result, increasing the power output of existing NPPs through power uprates has emerged as a more feasible and cost-effective strategy. One key area of advancement is the development of accident-tolerant fuel (ATF), such as chromium-coated zirconium alloy cladding, which offers enhanced material performance, enabling power uprates in light water reactors (LWRs).

Given the growing demand for nuclear energy fueled by federal policies and state initiatives, it is essential to evaluate the feasibility and benefits of significant power uprates in existing pressurized water reactors (PWRs) using advanced fuel technologies. The introduction of ATF concepts opens new opportunities for safely and economically achieving these power increases. Assessing whether these innovations can support substantial power uprates while maintaining operational safety is crucial to maximizing the potential of the nation's existing nuclear infrastructure.

This project aims to explore how power uprates can be achieved by boosting reactor thermal power output and optimizing reactor core design, while ensuring the safety and economic viability of NPPs. Specifically, it will focus on demonstrating the technical and economic feasibility of power uprates in a PWR using low 5-10% enrichment uranium (LEU+) high burnup (HBU) fuel combined with ATF concepts. In fiscal year 2024 (FY24), the research and development focus on building foundational models and conducting multi-physics performance and safety analyses to support the power uprate. The findings of the study would be shared through Light Water Reactor Sustainability seasonal meetings, conferences, and workshops with utility companies and researchers. These also serve as a basis for further study of fuel reloading optimization with ATF claddings.

Page intentionally left blank

CONTENTS

FIGURES

TABLES

Page intentionally left blank

ACRONYMS

ADF	assembly discontinuity factor
ATF	accident tolerant fuel
BOC	beginning of cycle
EOC	end of cycle
FY	fiscal year
FA	fuel assembly
HBU	high burnup
HE-LL-O	High Energy Low Leakage Optimized
HPI	high-pressure injection
IFBA	integral fuel burnable absorber
LEU+	low 5-10% enrichment uranium
LPI	low-pressure injection
LWR	light water reactor
NPP	nuclear power plant
NRC	Nuclear Regulatory Commission
PARCS	Purdue Advanced Reactor Core Simulator
PWR	pressurized-water reactor
RAVEN	Risk Analysis and Virtual Environment

Page intentionally left blank

1. INTRODUCTION

Demand for and advancements in nuclear technology in the United States (U.S.) have surged due to federal policy and state action in recent years. On November 15, 2021, President Biden signed the Infrastructure Investment and Jobs Act. This legislation makes significant investments in nuclear energy, allocating funds to preserve the operation of plants at risk of early closure, demonstrate advanced reactors, and explore nuclear energy's potential to produce hydrogen for other energy applications. The CHIPS and Science Act of 2022, signed on August 9, 2022, includes provisions supporting advanced nuclear energy technologies. The Inflation Reduction Act, signed on August 16, 2022, is anticipated to have a profound impact on the industry. It introduces a production tax credit for the existing nuclear fleet and clean electricity, an investment tax credit, and tax credits for hydrogen production. This legislation aims to preserve the existing fleet and create substantial future opportunities.

While building new nuclear power plants (NPPs), regardless of the technologies, often faces challenges associated with the cost and construction schedule, increasing the power output from existing NPPs creates a more realistic and cost-effective path to increase the installed nuclear capacity and thus the much-needed clean energy supply. The recent development of accident tolerant fuel (ATF) has made available a spectrum of advanced material, whether in the near term (e.g., coated Zr-alloy) or long term (e.g., SiC and FeCrAl cladding). Their superior material behavior and corrosion-resistant properties have the potential to allow power uprates in light water reactors (LWRs) beyond the current levels. They also require thorough and rigorous operational and safety analyses to understand the impacts. The main purpose of this project is to demonstrate technical and economic feasibility and expected benefits of power uprates.

Over the past few decades, there have been many power uprates approved by the U.S. Nuclear Regulatory Commission (NRC), resulting in a total increase of 22,560 MWth [1]. Historically, power uprates have been carried out in the U.S. in three different ways: measurement uncertainty recapture power uprates, stretch power uprates, and extended power uprates. Measurement uncertainty recapture power uprates consist of claiming a fraction of the 2% uncertainty factor to thermal power calculations specified in 10 CFR 50.62, Appendix K, to account for uncertainty in feedwater flow. This uncertainty reduction can result in an increase of reactor licensed thermal power between 1% and 2% and can be achieved by implementing improved thermal power calculation techniques. Stretch power uprates are typically between 2% and 7% and are achieved by making use of the original design's excess margins to accommodate an increase in thermal power. Extended power uprates refer to larger increases in thermal power beyond stretch power uprates. Extended power uprates require significant modifications to major balance-of-plant equipment, such as high-pressure turbines, condensate pumps and motors, main generators, and transformers.

There are several additional ways to support plant power increases, including the application of ATF, low 5-10% enrichment uranium (LEU+), risk-informed loss of coolant accident analysis, and extended fuel cycles. ATF can enhance safety at U.S. nuclear power plants by offering superior performance during normal operation, transient conditions, and accident scenarios. Combining these advanced fuel designs with increased enrichments up to 10% (LEU+) can boost operational flexibility, extend fuel cycles, and support power uprates. Risk-informed loss of cooling accident analysis provides a more accurate assessment of safety margins, incorporating probabilistic risk assessments to optimize safety measures and operational strategies. This analysis also helps identify and mitigate potential vulnerabilities, enhancing the reliability and efficiency of power uprates. Lastly, an extended fuel cycle supports power uprates by improving fuel efficiency and reducing refueling frequency. Utilizing HBU fuel and optimizing fuel management strategies allows the plant to sustain increased power levels for longer periods, minimizing operational interruptions, lowering fuel costs, and maximizing economic performance.

This project aims to conduct a feasibility study for a extended power uprate to a pressurized water reactor (PWR) by using low 5-10% enrichment uranium (LEU+) HBU fuel with ATF concepts. The safe operation of a NPP will be confirmed with appropriate system modifications to achieve economic benefits by leveraging near-term ATF concepts, such as Cr-coated Zr-alloy cladding. Performance and safety analyses of various power uprate approaches will be evaluated and compared in a multi-physics context, considering reactor physics, thermal-hydraulics, fuel performance, and economics, using state-of-the-art computational codes.

In FY24, research and development focused on establishing the foundation for assessing various sizable power uprate approaches. Baseline reactor core and system models were developed to facilitate reactor performance and safety analysis, based on the core model of a previously-collected design information of a 4-loop PWR reactor [2], henceforth referred to as the reference Pressurized Water Reactor (PWR). The Purdue Advanced Reactor Core Simulator (PARCS) [3], the U.S. NRC licensing tool for solving the time-dependent two-group neutron diffusion equation in three-dimensional Cartesian geometry, was employed to conduct calculations, ensuring the study's relevance to the nuclear industry and accelerating the licensing process with the identified optimal design approach. Fuel assembly models for the 17×17 fuel lattice were created to generate a multi-parameterized cross-section library. The core model was then developed, with cycle depletion results verified against those from SERPENT2 [4] to ensure the accuracy of the deterministic models. Additionally, a near-optimal equilibrium cycle of the reference PWR core was developed by a newly-created fuel shuffling scheme. The resulting equilibrium core meets the cycle energy production requirement (i.e., 18 months of cycle length) while satisfying various operational and safety limits, such as maximum discharge burnup, power peaking factors, and peak boron concentration. Lastly, a reactor system model was developed using RELAP5-3D. The reactor model is a typical four-loop PWR. The core model adopts the nodal kinetics calculation based on the NESTLE module. Neutron yields and cross-section data generated by POLARIS were transferred to this nodal kinetics module. A steady-state model was generated, and transient models are planned for development in the next fiscal year. Results of these transient analyses will inform if safe operation parameters are fulfilled in accident scenarios. Figure 1 shows the workflow of the project in FY24, with the dotted arrows indicating future planned work.

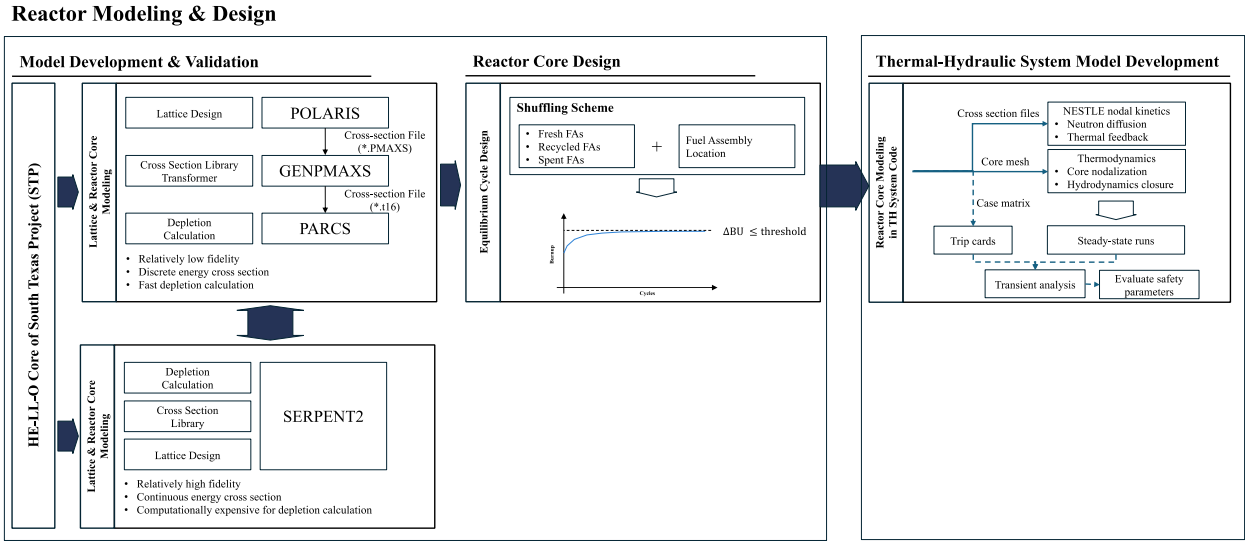

Figure 1. Workflow of the project in FY24. Dotted line in Thermal-Hydraulic System Model Development implies it is ongoing.

The rest of the report is organized in the following way: Section 2 provides detailed information on lattice and full core modeling in SERPENT2 and PARCS, along with a comparison of the results from both

models. Section 3 presents the RELAP5-3D system models of the reference PWR and briefly explains how the POLARIS cross-section results are integrated with the RELAP5-3D model. Section 4 concludes the study and outlines potential future work.

2. REACTOR CORE MODELING

SERPENT2 and PARCS are both widely used in reactor core modeling, but they serve different purposes and offer distinct advantages in terms of fidelity, computational cost, and application. SERPENT2 is a high-fidelity Monte Carlo code that provides detailed, accurate simulations of neutron transport. It models the behavior of neutrons within the reactor core with high spatial and energy resolution, making it capable of capturing complex phenomena with great precision. However, the downside of this high fidelity is the significant computational cost—SERPENT2 requires considerable processing power and time to run simulations, especially for full-core modeling. This makes it less practical for routine analyses or optimization studies that require quick turnaround times. PARCS, on the other hand, is a deterministic reactor core simulator that uses nodal methods to solve the neutron diffusion equation. While it operates with lower resolution compared to SERPENT2, PARCS is much faster and more computationally efficient. This makes it well-suited for large-scale, full-core simulations and iterative design tasks, such as core design optimization, equilibrium cycle modeling, and fuel management studies.

Performing comparative studies using both SERPENT2 and PARCS is important because it allows one to balance accuracy and efficiency. SERPENT2's high fidelity ensures that detailed physical phenomena are captured and can be used as a reference for validating other models. PARCS, with its lower computational demands, is ideal for routine analysis and optimization. By comparing results from both codes, we can ensure that the faster, more efficient PARCS simulations remain accurate and reliable, while using SERPENT2 to validate and improve the fidelity of lower-resolution models. This dual approach ensures that the benefits of both high-precision modeling and practical computational efficiency are realized.

In this study, the same fuel assemblies and full core model were developed and simulated in both SERPENT2 and PARCS for validation and comparison purposes. The full reactor core model was based on the reference PWR using publicly available documentation [2]. The reactor core design process involved two primary stages: lattice design and full core design. The lattice physics code, POLARIS [5], was used to model the 2D fuel assemblies at different axial positions. Reflector colorset models were generated to create the macroscopic cross-section libraries required for 3D full core modeling in PARCS [2]. The PARCS full core model was further utilized to refine the fuel shuffling scheme in the equilibrium cycle model. Additional details regarding the lattice and full core model specifications are provided in Appendix B.

2.1 Lattice Modeling

The lattice code POLARIS was used to model the lattice physics and generate the macroscopic cross sections for the 3D full core model. These models were also generated in SERPENT2 to validate the resulting cross section libraries between the two codes. This included considerations for the several fuel assembly designs and axial regions to be used in the full core, as well as the axial and radial reflectors.

2.1.1 Fuel Assemblies Modeling

The fuel assemblies were modeled both in POLARIS and SERPENT2, and the results were compared for all the fuel assemblies considered for the core design. Fuel assembly design used in the report is shown in Figure 2. The total fuel assembly's active height is 14 feet, of which 8 inches from the top and the bottom are blanket regions with 2.6 w.t.% 235U enrichment. The fuel assemblies contain three different enrichment regions in active height, one containing the assembly's active fuel nominal enrichment, and one each on the top and bottom of the fuel assembly containing the reduced enrichment

blanket regions. These axial regions containing different fuel enrichments and types were modeled separately in POLARIS.

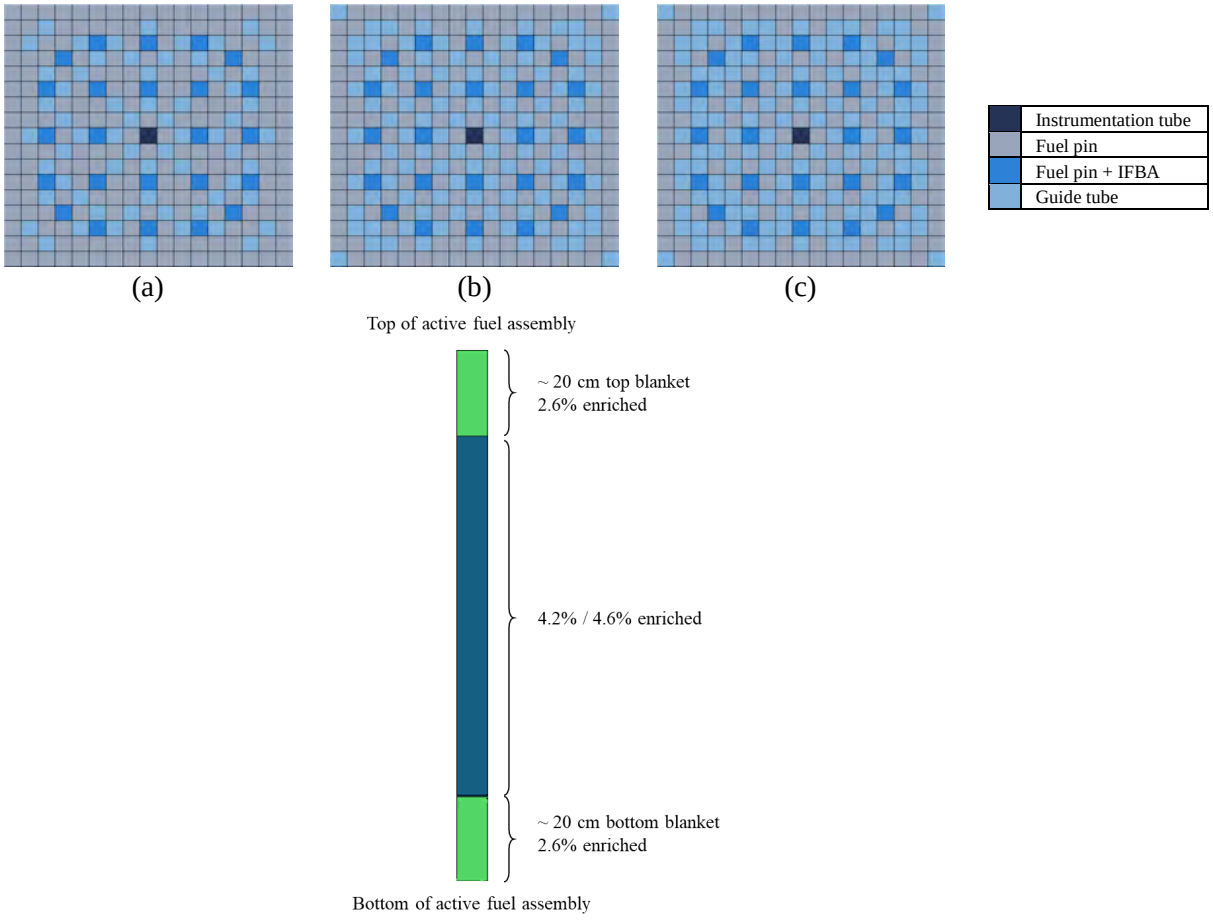

Figure 2. Radial layout of components in 17×17 Fuel Assemblies [6]: (a) 64 IFBA, (b) 108 IFBA, (c) 128 IFBA. and (d) axial enrichment regions in fuel assemblies.

Figure 3 illustrates the geometric and material specifications for the fuel pin, empty guide tube, control rod within the guide tube, and fuel pin containing burnable poison. The specifications for the fuel assemblies are detailed in Table 1.

Table 1. Fuel assembly specifications.

Specification	Value
Fuel rod array	17 × 17
UO_2 rods	264
Guide Tubes	24
Instrumentation Tubes	1
Fuel density (g/cc)	10.412
Assembly pitch (cm)	21.50
Rod pitch (cm)	1.26

Overall dimensions (cm × cm)	21.402 × 21.402

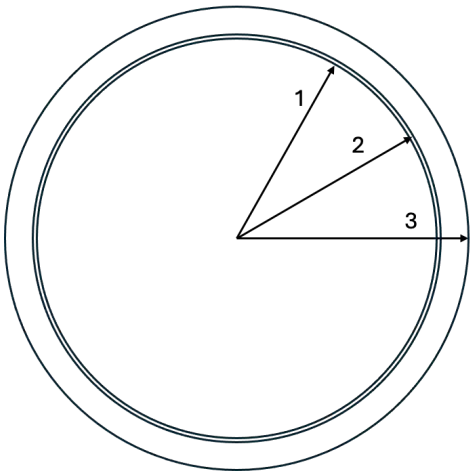

Fuel Pin Part	Radius (cm)	Material
1	0.4096	UO_2
2	0.4178	Helium
3	0.4750	ZIRLO

(a)

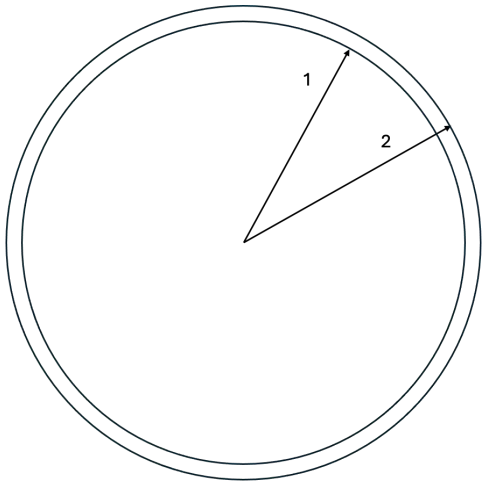

Empty guide tube	Radius (cm)	Material
1	0.5715	Water Coolant
2	0.6120	ZIRLO

(b)

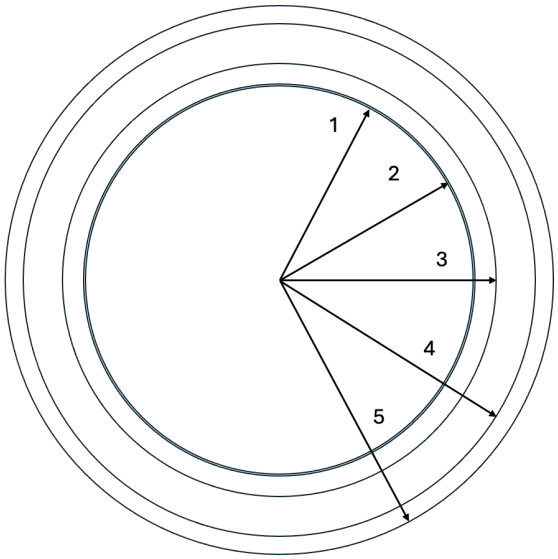

Control Rod in Guide tube	Radius (cm)	Material
1	0.4331	Ag-In-Cd
2	0.4369	Helium
3	0.4839	SS304
4	0.5715	Water Coolant
5	0.6120	ZIRLO

(c)

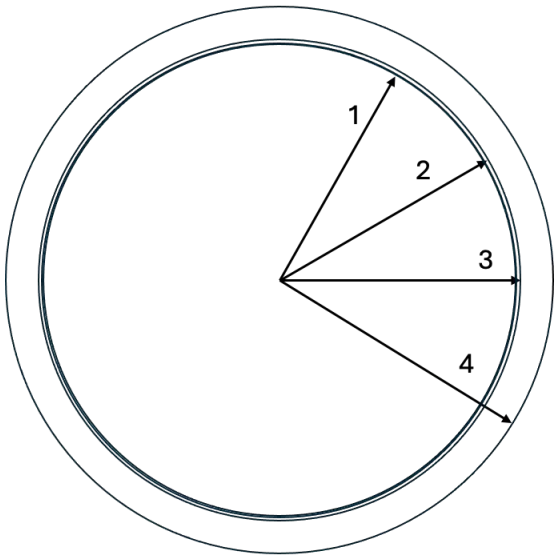

Fuel pin with burnable poison	Radius (cm)	Material
1	0.4096	UO_2
2	0.4122	IFBA
3	0.4178	Helium
4	0.475	ZIRLO

(d)

Figure 3. Geometric and material specifications used in fuel assemblies: (a) Fuel pin; (b) Empty guide tube; (c) Control Rod in Guide tube; and (d) Fuel pin with burnable poison.

Table 2 shows four different fuel assembly types modeled in this study. Three were loaded with 4.2 w.t.% UO2 fuel in the active fuel region with differing configurations of integral fuel burnable absorber (IFBA) rods, containing a total of 64, 104, and 128 IFBA rods, respectively. The fourth fuel assembly type was loaded with 4.6 w.t.% UO_2 fuel in the active fuel region and 128 IFBA rods. All four fuel assembly types were otherwise identical in geometry, utilizing the same specifications of rod diameter, pitch, and height and configuration of guide or instrumentation tubes, as shown in Figure 3.

Table 2. Fuel assembly types used in the HE-LL-O core model [6]. Assembly ID is used for shuffling scheme in Figure 19.

Assembly (ID)	Enrichment (wt.%)	Burnable poison loading (IFBA)
A194	4.2	64
A195	4.2	104
A196	4.2	128
A197	4.6	128

After completing lattice modeling, depletion calculations were conducted for the blanket regions and each of the four fuel assembly types. Figure 4 shows a comparison of the resulting k-infinite values as a function of burnup for the POLARIS and SERPENT2 models across all fuel assembly types, including the blanket region. The k-infinite profiles across the burnup rate from PARCS and SERPENT2 align closely, indicating a good match.

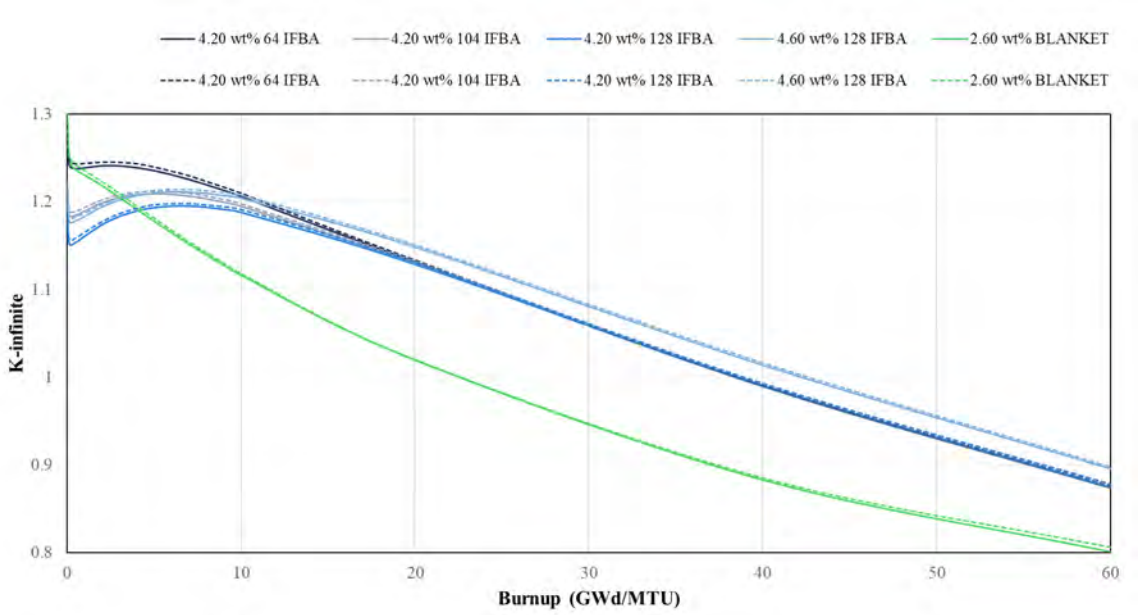

Figure 4. K-effective vs. burnup curves for the different fuel assemblies modeled in SERPENT2 and POLARIS.

To further verify the agreement between these two codes, the difference between POLARIS and SERPENT models was also illustrated, as shown in Figure 5. The comparison shows good agreement

between the two models within an acceptable range, with an average difference between the POLARIS and SERPENT2 models of 362.24 pcm.

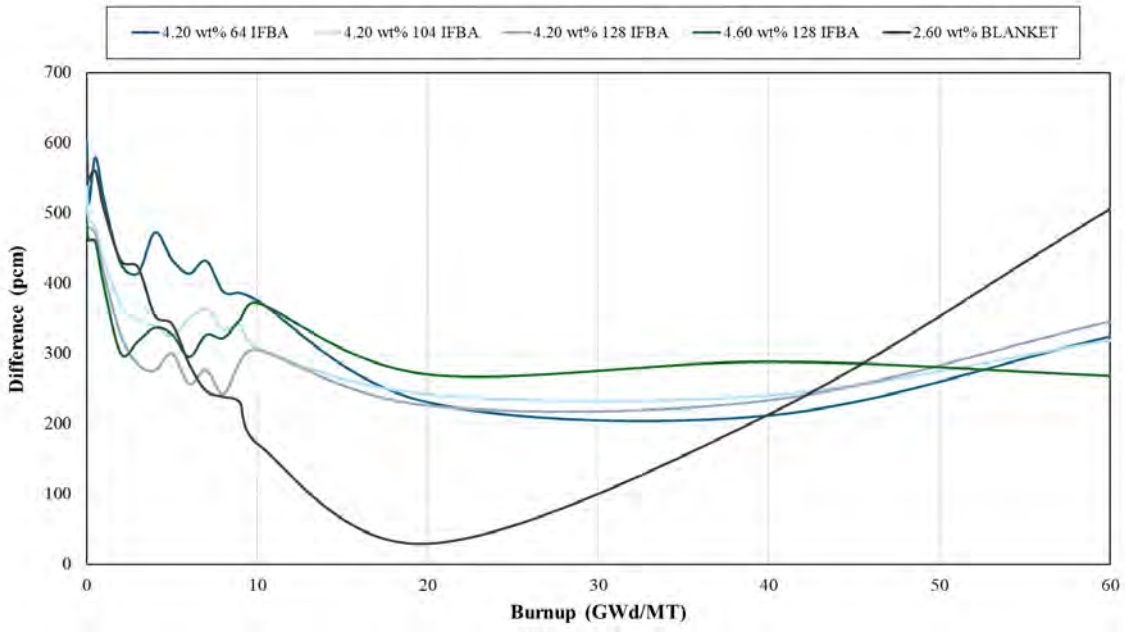

Figure 5. Difference in pcm (10E-5) between the models generated in SERPENT2 and POLARIS.

2.1.2 Reflectors Modeling

The modeling of reflectors requires a colorset model that includes the reflector region and an adjacent fuel assembly. In nuclear reactor core design, a "colorset" model is a simplified representation used to simulate a portion of the reactor core rather than the entire core. The colorset approach divides the reactor core into symmetrical segments or "colors," where each color represents a specific repeating pattern of fuel assemblies and control elements. These patterns are then modeled independently to gain insights into the reactor's behavior without needing to simulate the entire core. The colorset model takes advantage of the symmetry in the core to reduce the computational complexity of simulations. By focusing on a single segment, or "colorset," and applying boundary conditions that reflect the symmetrical nature of the core, one can predict how the full core will perform under various conditions. POLARIS offers the capability to model reflectors by using two identically-sized blocks to capture the boundary between the reflector region and neighboring fuel assembly, where we can individually define the boundary condition for each side. To validate results from the POLARIS model, a SERPENT2 model with identical geometry and similar boundary conditions was developed.

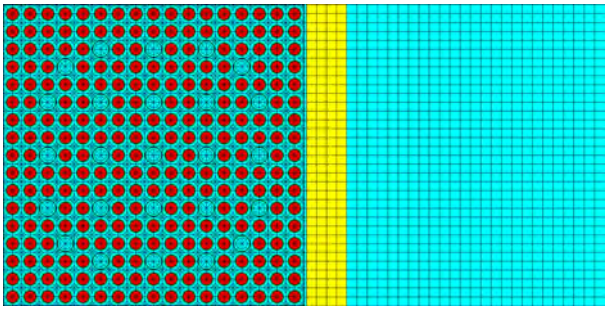

Figure 6. POLARIS reflector colorset model. Red-colored circle is fuel pin; circle without red color is either guide tube or instrumentation tube; yellow color is reflector baffle; and light blue color is coolant (water).

A fuel assembly of 4.2% enrichment was used as the driver for the colorset model. Since defining independent boundary conditions in the same direction in SERPENT2 is not possible, three different approaches were explored to approximate the SERPENT2 reflector model to the one in POLARIS. To compare the results, 2-group macroscopic cross section values for total, capture, diffusion coefficient, transport, and assembly discontinuity factor (ADF) were calculated and compared between POLARIS and the three models. Table 3 shows the difference of boundary conditions between POLARIS and SERPENTS.

Table 3. Boundary conditions of colorset models in SERPENT2 and POLARIS.

		East BC	**West BC**	**North BC**	**South BC**	**Modeling Features – East BC in SERPENT2**
POLARIS	Baseline	Black	Reflective	Reflective	Reflective	-
SERPENT2	Approach 1	Reflective				Standard Reflector
	Approach 2					Long Reflector
	Approach 3					Standard Reflector + Absorbent block

BC: Boundary Condition

The first approach is to model two adjacent blocks of the same size: one containing the fuel assembly, and the other the reflector region. The boundary conditions are reflective in all four directions. Table 4 shows comparison results of a macroscopic cross-section of Approach 1 in the reflector region (i.e., blue colored coolant region next to grey-colored cladding region). Cross-sections were generated for two macroscopic groups divided at 0.625 eV, Group 1 and Group 2. It is important to note that most cross-section results, except for the capture cross-section, were closely aligned. The ADF results in Group 2 exhibited a significant difference, with approximately a 10% error. The relative error between the SERPENT2 and POLARIS was calculated using Equation (1):

$$\text{Relative error (\%)} = \frac{\text{SERPENT2} - \text{POLARIS}}{\text{SERPENT2}} \times 100 \quad (1)$$

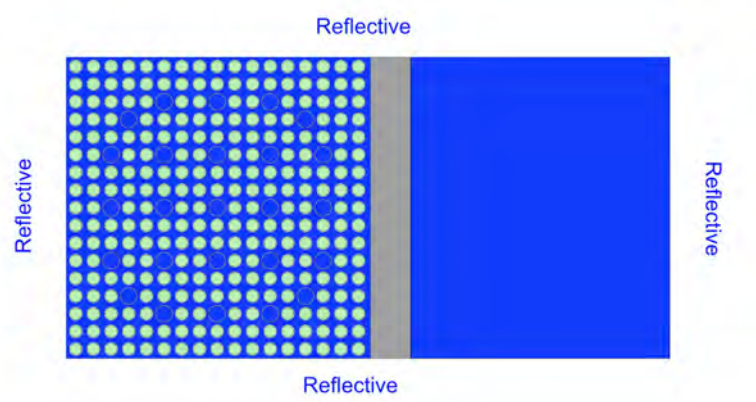

(a)

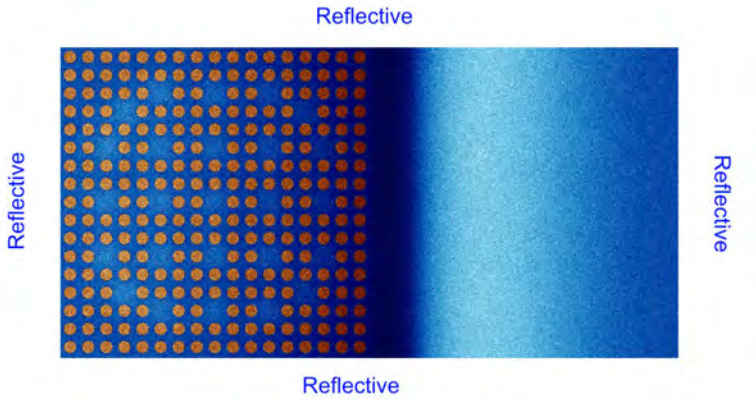

(b)

Figure 7. (a) Colorset model of fuel assembly and reflector – standard reflector region in SERPENT2. (b) Neutron flux in fuel assembly and reflector. The light contrast indicates high intensity of neutron flux.

Table 4. Comparison of Macroscopic Cross-section of Approach 1– POLARIS vs. SERPENT2.

Reflector	**Parameter**	**POLARIS**	**SERPENT2**	**Rela. Error (%)**
Group 1	Total [1/cm]	0.63462	0.63934	0.73764
	Capture [1/cm]	0.00152	0.00197	22.57520
	Diff Coeff. [cm]	1.34214	1.32595	-1.22101
	Transport [1/cm]	0.24836	0.25140	1.20844
	ADF	0.97451	1.02005	4.46449
Group 2	Total [1/cm]	1.84173	1.86007	0.98598
	Capture [1/cm]	0.01769	0.01562	-13.27416
	Diff Coeff. [cm]	0.28164	0.27717	-1.61200
	Transport [1/cm]	1.18354	1.20262	1.58654
	ADF	0.19669	0.21839	9.93676

The second approach to modeling the reflector in SERPENT2 is using a longer reflector region, as shown in Figure 8. In this approach, the extended reflector region is filled with water for an extra 21.50 cm. Table 5 shows comparison results of the macroscopic cross-section of Approach 2 in the reflector region (i.e., blue colored coolant region next to grey-colored cladding region). A similar pattern has been observed in cross-section data: except for the capture cross-section, the results from both POLARIS and SERPENT2 models are well aligned. The ADF results in Group 2 also exhibited a certain degree of difference, with approximately 7% error.

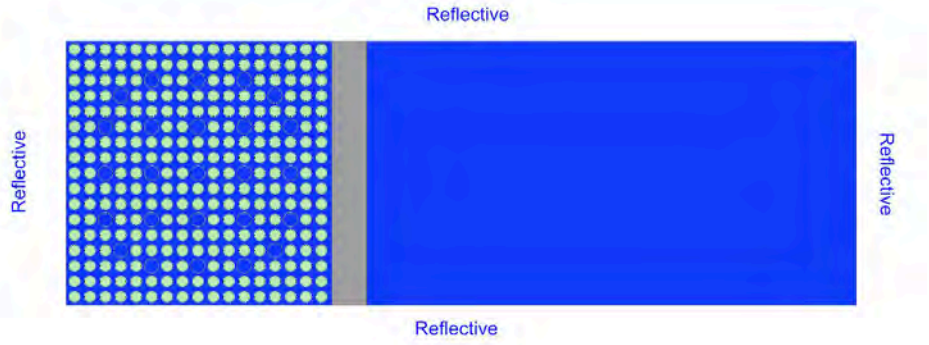

(a)

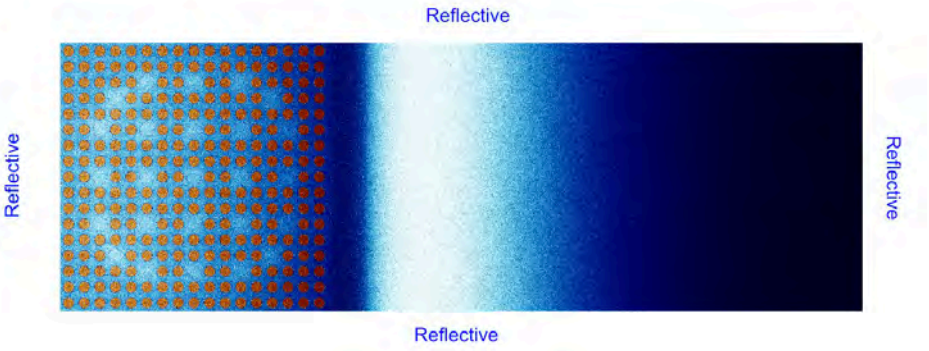

(b)

Figure 8. (a) Colorset model of fuel assembly and reflector – long reflector region in SERPENT2. (b) Neutron flux in fuel assembly and reflector. The light contrast indicates high intensity of neutron flux.

Table 5. Comparison of Macroscopic Cross-section of Approach 2– POLARIS vs. SERPENT2.

Reflector	Parameter	POLARIS	SERPENT2	Rela. Error (%)
Group 1	Total [1/cm]	0.63462	0.64056	0.93568
	Capture [1/cm]	0.00152	0.00203	32.85118
	Diff Coeff. [cm]	1.34214	1.30135	3.03918
	Transport [1/cm]	0.24836	0.25615	3.13617
	ADF	0.97451	0.99638	2.24379
Group 2	Total [1/cm]	1.84173	1.85299	0.61138
	Capture [1/cm]	0.01769	0.01638	7.42612
	Diff Coeff. [cm]	0.28164	0.27785	1.34427
	Transport [1/cm]	1.18354	1.19967	1.36286
	ADF	0.19669	0.18364	6.63684

A third approach to model the reflector is to try to approximate the black boundary condition by using a high neutron absorbing material. For this purpose, a hafnium block was modeled in the far right of our reflector model. Table 6 shows comparison results of the macroscopic cross-section of Approach 3 in the reflector region (i.e., blue colored coolant region next to grey-colored cladding region). Again, a similar pattern has been observed in cross-section data: except the capture cross-section, results from both POLARIS and SERPENT2 models are well aligned. The ADF results in Group 2 showed a relatively smaller difference compared to Approaches 1 and 2, with an error of approximately 4.8%.

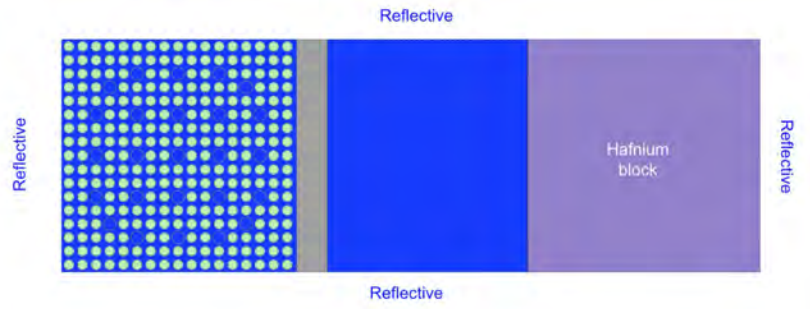

(a)

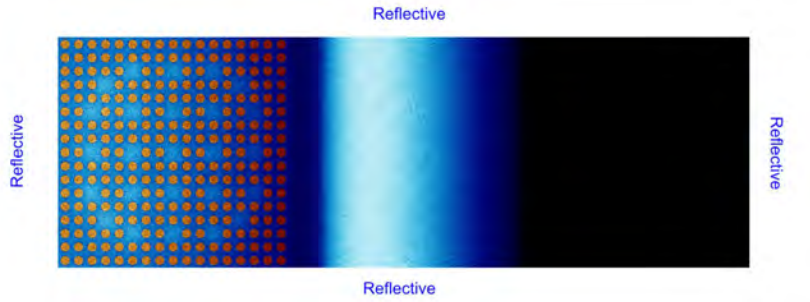

(b)

Figure 9. (a) Colorset model of fuel assembly and reflector – standard reflector with absorbent block in SERPENT2. (b) Neutron flux in fuel assembly and reflector. The light contrast indicates high intensity of neutron flux.

Table 6. Comparison of Macroscopic Cross-section of Approach 3 – POLARIS vs. SERPENT2.

Reflector	Parameter	POLARIS	SERPENT2	Rel Error (%)
Group 1	Total [1/cm]	0.63462	0.64188	1.13105
	Capture [1/cm]	0.00152	0.00201	24.08888
	Diff Coeff. [cm]	1.34214	1.30036	3.21296
	Transport [1/cm]	0.24836	0.25634	3.11419
	ADF	0.97451	0.99776	2.32983
Group 2	Total [1/cm]	1.84173	1.84768	0.32203
	Capture [1/cm]	0.01769	0.0169	4.69655
	Diff Coeff. [cm]	0.28164	0.27845	1.14490
	Transport [1/cm]	1.18354	1.19709	1.13191
	ADF	0.19669	0.18764	4.82418

We can see in Table 6 that in the three approaches, the cross-sections generated in SERPENT2 and POLARIS are generally in good agreement, with the exception of the capture cross-section. Table 7 shows summarized results of a comparison focusing only on the capture cross-section for the three approaches. SERPENT2 is a Monte Carlo code, the reason why its results come with an intrinsically statistical error.

Table 7. Summary of comparison of macroscopic capture cross section in the POLARIS model and three different SERPENT2 models.

	Group	POLARIS	SERPENT2	Relative Error (%)	Std.	SERPENT2 Range	POLARIS in SERPENT2 Range
Standard reflective	1	0.00152	0.00197	22.575	± 0.001	0.00033 - 0.00361	Yes
	2	0.01769	0.01562	13.2742	± 0.0006	0.01502 - 0.01622	No
Long reflective	1	0.00152	0.00203	32.8512	± 0.0016	0.00042 - 0.00364	Yes
	2	0.01769	0.01638	7.4261	± 0.0007	0.01571 - 0.01705	No
Standard reflective+ Hafnium Block	1	0.00152	0.00201	24.0889	± 0.0014	0.00058 - 0.00344	Yes
	2	0.01769	0.01690	4.6966	± 0.0009	0.01603 - 0.01777	Yes

2.1.3 Cross Section Generation

The cross section libraries were generated using the lattice physics code POLARIS. Once validated against the SERPENT2 models, each type of fuel assembly described previously was modeled as a 2D lattice under various conditions of fuel and coolant temperature, coolant density, boron concentration, and control rod insertion to capture the range of conditions in each of these state variables that might be expected during nominal operation or could arise as the result of safety-related transients. At each set of conditions, macroscopic multi-group cross sections for the homogenized fuel assembly were generated and concatenated to form a complete case matrix cross section library. The extent of perturbed values for each state variable is summarized in Table 8.

Table 8. Perturbation values included in the POLARIS case matrix cross section library.

State Variable	Values				
Fuel Temperature (K)	560	900	1200	2000	
Coolant Density (g/cm^3)	0.102	0.200	0.450	0.653	0.740
Boron Concentration (PPM)	0	500	1500		
Control Rods Inserted	Fully Removed	Fully Inserted			

Each perturbed value for fuel temperature, coolant density, and boron concentration was treated as a single-parameter perturbation of the nominal case, resulting in 12 unique cases. These were then repeated with the "control rods fully inserted" perturbed value applied, resulting in an additional 12 unique cases, or 24 cases in total. Each case included 20 depletion timesteps to a total burnup of 65 GWd/MTU at a nominal reactor power of 36 W/g_{IHM}.

The cross sections were generated in POLARIS using nuclear data taken from a 252-group library derived from the ENDF/B VII.1 database. These are generated in the '.t16' file format as 2-group macroscopic cross sections in the '.PMAXS' file format using the code GenPMAXS, allowing for use in PARCS and RELAP5-3D.

2.1.4 Axial Discontinuity Factors (ZDF)

Given that the blankets have a different enrichment compared to the nominally enriched regions in the fuel assemblies, an inspection of the axial discontinuity factors (ZDF) was conducted. Axial discontinuity factors were calculated for fuel assembly A195, with an enrichment of 4.2 wt% and 104 IFBA. Nodes were placed at every foot along the axial position, and ZDFs were determined for both the top and bottom of each node. Since the blankets occupy the top and bottom 8 inches of the assembly, additional nodes were also added specifically for the blanket regions. The ZDF values for positions at the top of the node are expressed as T1 and T2 for macro groups 1 and 2 respectively. Similarly, ZDF values at the bottom of the nodes are expressed as B1 and B2. ZDF values for the blanket nodes are also specified.

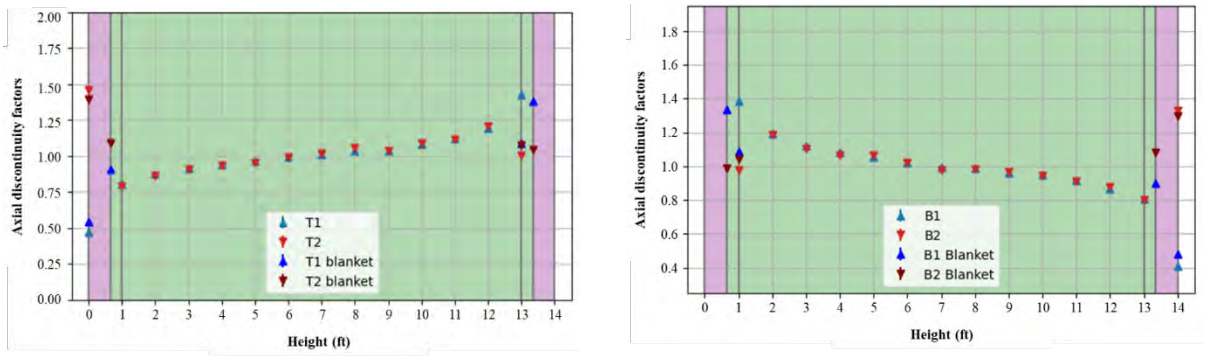

(a) (b)

Figure 10. Axial discontinuity factor changes in heterogeneous fuel assembly – (a) at the top of cell. (b) at the bottom of cell.

2.2 Full Core Modeling

A 15 × 15 fuel assembly core was modeled as a 3D full core using both PARCS and SERPENT2, based on publicly available data from the reference PWR [2]. The SERPENT2 model was developed to validate the PARCS model and assess the impact of axial heterogeneity introduced by the blankets in the fuel assemblies. For comparison, both models were created to be as similar as possible; however, some differences remain due to the inherent characteristics and limitations of the two codes. Key differences include the treatment of cross-section libraries, the level of detail in geometry definition, and the stochastic nature of the Monte Carlo method in SERPENT2 versus the deterministic approach used in PARCS.

Table 9. Specifications of HE-LL-O Core of the reference PWR [2] [6].

Specification	Value
Core dimensions	15 assemblies across
Active height (cm)	426.72
Thermal power (MWth)	3411
Operating pressure (psia)	2250
Inlet Temperature (F)	566

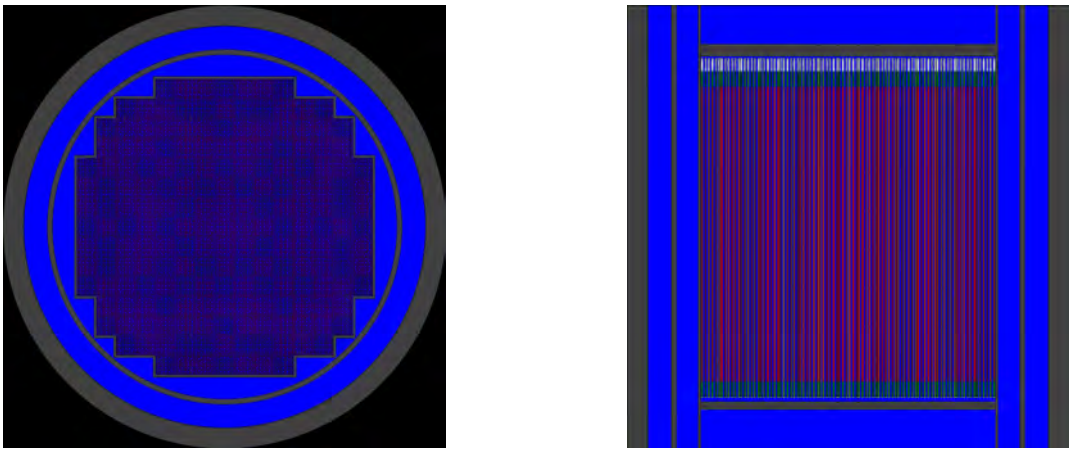

(a) (b)

Figure 11. Radial and axial views of HE-LL-O model in SERPENT2. a) Top view of reactor core, b) cross section view of reactor core.

2.2.1 Development of Steady State Model

As an initial step toward full core reactor design, a steady-state core using fresh fuel was modeled. The loading pattern was inspired by the modeling results of the HE-LL-O core design [2]. In this model, each assembly was treated as fresh fuel for simplicity, resulting in a core configuration with an unrealistically high level of excess reactivity. It served as a practical baseline for comparison between the PARCS and SERPENT2 models.

	A	B	C	D	E	F	G	H	J	K	M	N	P	Q	R
1					128A	128	128	128A	128	128	128A				
2			128A	128	64	128A	128A	128	128A	128A	64	128	128A		
3		128A	64	104	128	128	104	128A	104	128	128	104	64	128A	
4		128	104	128	128A	104	128	104	128	104	128A	128	104	128	
5	128A	64	128	128A	104	128A	104	128A	104	128A	104	128A	128	64	128A
6	128	128A	128	104	128A	104	128A	64	128A	104	128A	104	128	128A	128
7	128	128A	104	128	104	128A	64	104	64	128A	104	128	104	128A	128
8	128A	128	128A	104	128A	64	104	**128**	104	64	128A	104	128A	128	128A
9	128	128A	104	128	104	128A	64	104	**64**	128A	104	128	104	128A	128
10	128	128A	128	104	128A	104	128A	64	128A	**104**	128A	104	128	128A	128
11	128A	64	128	128A	104	128A	104	128A	104	128A	**104**	128A	128	64	128A
12		128	104	128	128A	104	128	104	128	104	128A	**128**	104	128	
13		128A	64	104	128	128	104	128A	104	128	128	104	**64**	128A	
14			128A	128	64	128A	128A	128	128A	128A	64	128	128A		
15					128A	128	128	128A	128	128	128A				

	Enrichment	# IFBA
64	4.2 w.t.%	64
104	4.2 w.t.%	104
128	4.2 w.t.%	128
128A	4.6 w.t.%	128

Figure 12. Loading pattern used for the steady state modeling of HE-LL-O core design.

K-eigenvalue calculations were performed in both PARCS and SERPENT2 using this steady state loading pattern to validate the relative performance between the two models. The steady state calculation in PARCS took 3.79 seconds on 1 CPU, or 0.00105 CPU-hrs., and 41 min 56 seconds on 32 CPUs, or 0.02184 CPU-hrs. in SERPENT2 using a population of 1,000,000 neutrons with 160 active cycles and 50 inactive cycles.

Figure 13 illustrates the radial power distribution for a quarter-sized core and the corresponding error comparison between the SERPENT2 and PARCS models. The relative error between the SERPENT2 and PARCS was calculated with Equation (2). The macroscopic cross-section library used in PARCS was generated in POLARIS as described previously, using the ENDF/B VII.1 microscopic cross section libraries. SERPENT2 modeled also used ENDF/B VII.1, however, the thermal scattering cross sections were taken from ENDF/B VII due to availability.

2.99	3.00	2.69	1.96	1.39	0.93	0.55	0.25
2.89	2.95	2.69	1.99	1.39	0.95	0.55	0.25
3.01	2.95	2.43	1.86	1.31	0.90	0.54	0.24
2.95	2.95	2.45	1.85	1.30	0.91	0.55	0.23
2.69	2.44	2.05	1.60	1.17	0.79	0.49	0.22
2.69	2.45	2.04	1.63	1.18	0.78	0.50	0.21
1.97	1.86	1.60	1.30	0.96	0.66	0.42	0.16
1.99	1.85	1.63	1.31	0.98	0.65	0.42	0.16
1.40	1.30	1.17	0.96	0.73	0.51	0.27	
1.39	1.30	1.18	0.98	0.71	0.51	0.26	
0.94	0.89	0.79	0.66	0.51	0.36	0.16	
0.95	0.91	0.78	0.65	0.51	0.35	0.15	
0.56	0.54	0.49	0.42	0.27	0.15		
0.55	0.55	0.50	0.42	0.26	0.15		
0.25	0.24	0.22	0.16				
0.25	0.23	0.21	0.16				

Serpent
PARCS

(a)

3.21	1.69	0.20	1.32	0.27	2.30	0.81	0.21
1.89	0.01	0.74	0.16	0.53	1.02	2.80	3.46
0.02	0.33	0.62	2.24	1.14	0.70	1.81	4.52
0.99	0.52	2.22	0.51	2.25	1.82	0.55	3.60
0.11	0.45	1.04	2.44	1.63	0.90	5.66	
1.60	1.17	0.40	1.14	1.03	1.58	6.36	
2.68	1.36	1.26	0.35	5.77	5.43		
1.73	4.81	5.04	3.15				

(b)

Figure 13. (a) Relative radial power distribution in SERPENT2 and PARCS and (b) Relative error map.

$$\text{Relative error (\%)} = \frac{\text{abs}|\text{SERPENT2} - \text{PARCS}|}{\text{SERPENT2}} \times 100 \quad (2)$$

Given the statistical nature of SERPENT2, the mean values of the radial power distribution were used in the above formula for simplicity. For the radial power distribution steady state models, the relative error between the two models is about 1.80%, with 6.36% being the maximum relative error in a fuel assembly. We can see that the error is greater by the periphery, which can be explained by intrinsic differences in how the reflectors are modeled in SERPENT2 and PARCSS and the use of different thermal scattering cross section libraries used by the two models.

The axial power was also compared between the two models. The average relative error between the two models is 2.74%, with a maximum error of 6.78%. Some key factors that may explain the differences between the two models include the level of geometric detail, the inherent nature of the codes, and the use of different thermal scattering cross-section libraries.

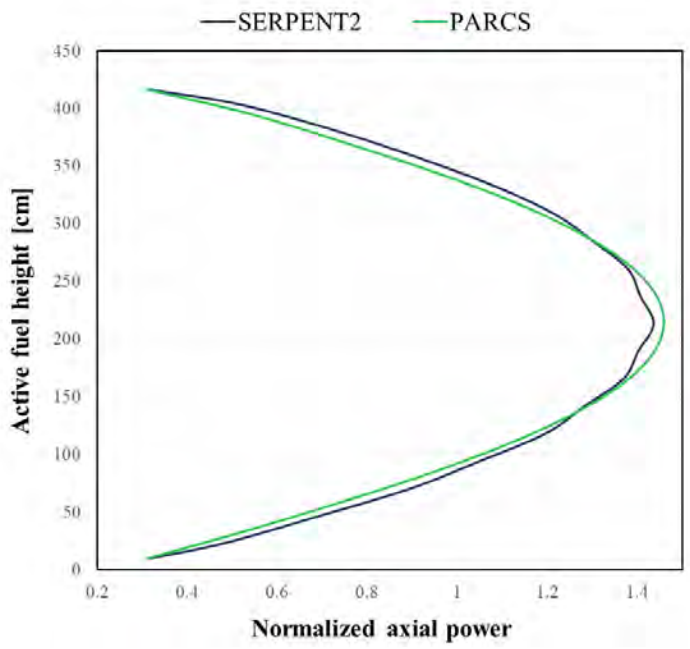

Figure 14. Axial power distribution comparison of the SERPENT2 and PARCS models.

2.2.2 Depletion Calculation

To assess the impact of axial heterogeneity introduced by the blanket regions in the fuel assemblies, a comparison of depletion calculation was conducted in SERPENT2 between a model with axially homogeneous fuel assemblies (without blankets) and a model with axially heterogeneous assemblies (with blankets) using the loading pattern described in Figure 12.

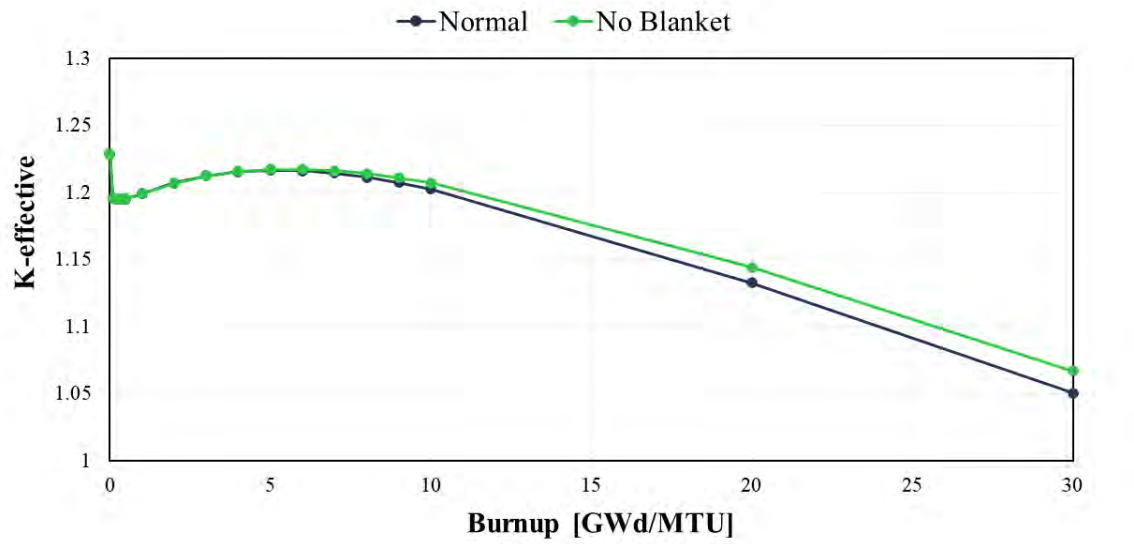

Figure 15. K-effective profiles as a function of burnup rate with and without the blanket.

Figure 15 shows K-effective profiles as a function of burnup rate with and without the blanket. The difference between the models is not significant and remains below 1643 pcm.

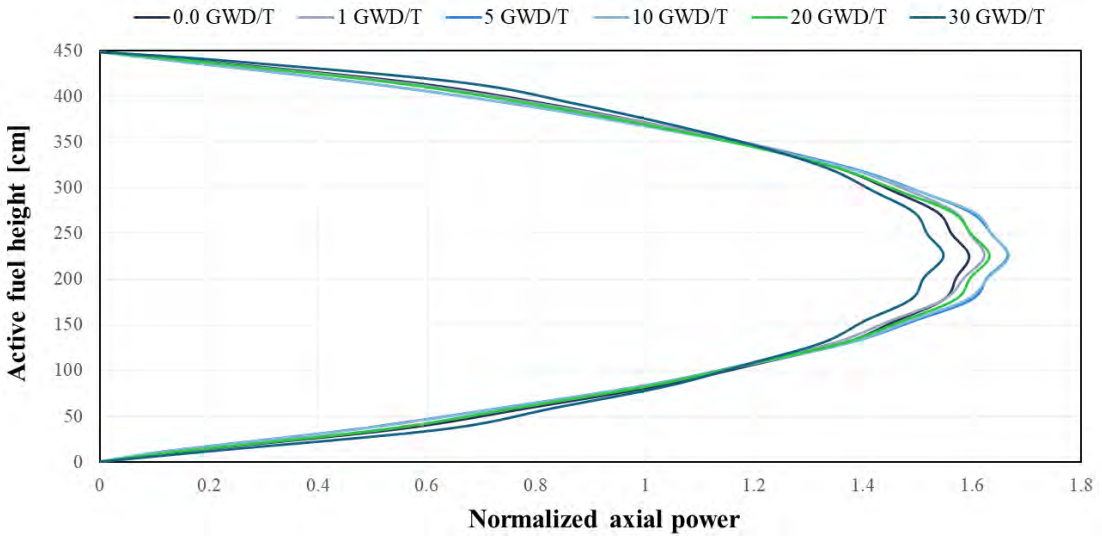

Figure 16. Axial power distribution against different burnup steps.

Figure 16 shows axial power distribution against different burnup steps. We can appreciate the flattening of the axical power profile in the latter burnup steps.

	A	B	C	D	E	F	G	H	J	K	M	N	P	Q	R
1					128A	128	128	128A	128	128	128A				
2			128A	128	64	128A	128A	128	128A	128A	64	128	128A		
3		128A	64	104	128	128	104	128A	104	128	128	104	64	128A	
4		128	104	128	128A	104	128	104	128	104	128A	128	104	128	
5	128A	64	128	128A	104	128A	104	128A	104	128A	104	128A	128	64	128A
6	128	128A	128	104	128A	104	128A	64	128A	104	128A	104	128	128A	128
7	128	128A	104	128	104	128A	64	104	64	128A	104	128	104	128A	128
8	128A	128	128A	104	128A	64	104	**128**	104	64	128A	104	128A	128	128A
9	128	128A	104	128	104	128A	64	104	**64**	128A	104	128	104	128A	128
10	128	128A	128	104	128A	104	128A	64	128A	**104**	128A	104	128	128A	128
11	128A	64	128	128A	104	128A	104	128A	104	128A	**104**	128A	128	64	128A
12		128	104	128	128A	104	128	104	128	104	128A	**128**	104	128	
13		128A	64	104	128	128	104	128A	104	128	128	104	**64**	128A	
14			128A	128	64	128A	128A	128	128A	128A	64	128	128A		
15					128A	128	128	128A	128	128	128A				

	Enrichment	# IFBA
64	4.2 w.t.%	64
104	4.2 w.t.%	104
128	4.2 w.t.%	128
128A	4.6 w.t.%	128

Figure 17. Loading pattern used for the steady state modeling of HE-LL-O core design without burnable poison.

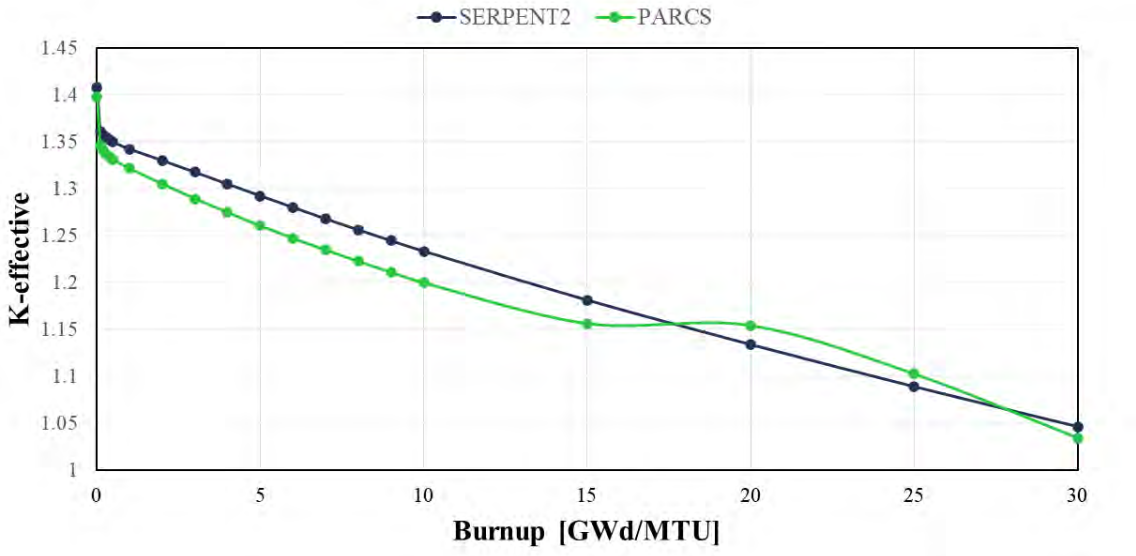

Figure 18. Comparison of K-effective profile changes against burnup rate between SERPENT2 and PARCS – without burnable poison.

Figure 18 shows comparative results of K-effective profile changes against burnup rate between SERPENT2 and PARCS. A depletion of the first cycle was made using the loading pattern shown in Figure 17. Considering the minor effect coming from the heterogeneity in blankets, the ZDFs were not

used in the PARCS model. The difference ranges between 1003 and 3363 pcm with an average of 2352 pcm.

2.3 Equilibrium Cycle Modeling

The equilibrium cycle was modeled as a 3D full core using PARCS with cross section libraries created in POLARIS. This model was inspired by the HE-LL-O shuffling scheme of the 14' reference PWR reactor design. The feed batch size (batch 1) is 72 assemblies, all of which are reloaded as once-burned fuel assemblies in batch 2. Batch 3 consists of 49 twice-burned fuel assemblies, selected from batch 2. The full shuffling scheme for this equilibrium cycle detailing these reloading motions is depicted in Figure 18.

	A	B	C	D	E	F	G	H	J	K	M	N	P	Q	R
1					F3	F5	G4	D5	J4	K5	K3				
2			G3	F1	A194	A197	A197	H7	A197	A197	A194	K1	J3		
3		C7	A194	A195	E4	E2	G6	C3	J6	M2	J2	A195	A194	P7	
4		A6	A195	H1	A196	G2	A196	F2	A196	N3	A196	R8	A195	R6	
5	C6	A194	B7	A196	A7	A196	H2	D3	M8	A196	J1	A196	N5	A194	P6
6	E6	A197	B5	C4	A196	H6	A196	B6	A196	K8	A196	Q7	Q5	A197	M6
7	D7	A197	F7	A196	H5	A196	G1	A196	R7	A196	Q8	A196	K7	A197	N7
8	E12	G8	C13	B10	C12	F14	A196	H13	A196	K2	P4	Q6	P3	J8	M4
9	D9	A197	F9	A196	B8	A196	A9	A196	J15	A196	H11	A196	K9	A197	N9
10	E10	A197	B11	B9	A196	F8	A196	Q10	A196	H10	A196	P12	Q11	A197	M10
11	C10	A194	D11	A196	G15	A196	E8	N13	H14	A196	R9	A196	Q9	A194	P10
12		A10	A195	A8	A196	D13	A196	K14	A196	J14	A196	H15	A195	R10	
13		C9	A194	A195	G14	E14	G10	P13	J10	M14	M12	A195	A194	P9	
14			G13	F15	A194	A197	A197	H9	A197	A197	A194	K15	J13		
15					F13	F11	G12	N11	J12	K11	K13				

Key	Description
A194	4.2 w.t.% + 64 IFBA
A195	4.2 w.t.% + 104 IFBA
A196	4.2 w.t.% + 128 IFBA
A197	4.6 w.t.% + 128 IFBA
OB	Once burned
TB	Twice burned

Figure 19. The reference PWR Equilibrium Cycle Shuffling Scheme

Xenon and Samarium were assumed to be at equilibrium throughout the depletion calculations. Control rod bank positions were kept fully withdrawn for these calculations. The PARCS model of this shuffling scheme as an equilibrium cycle converged in nine repeated cycles with a constant fuel temperature of 900°C. The convergence of the calculation in PARCS and validation of this shuffling scheme as an equilibrium cycle is demonstrated through the convergence of the EOC core-averaged burnup through repeated cycles, as depicted in Figure 19.

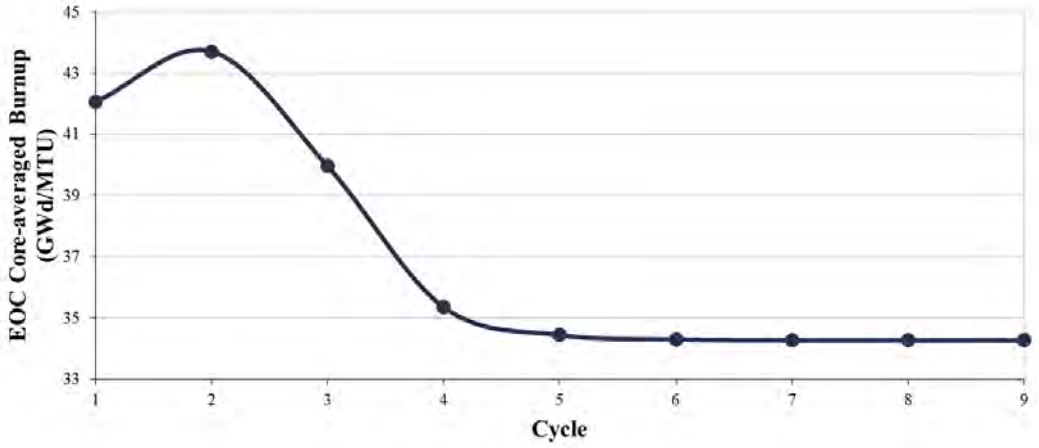

Figure 20. Convergence of EOC core-averaged burnup verifying equilibrium behavior.

Using the design depicted in Figure 18, the length of the fuel cycle has been extended to 530 effective full power days, resulting in a peak soluble boron concentration of 1293.4 ppm, a maximum 3D nodal burnup of 62.6 GWd/TU, and thermal peaking factors of F_q = 1.882 and $F_{\Delta H}$ = 1.463. The behavior of this equilibrium cycle is demonstrated in the depletion curves of core average exposure and change in soluble boron concentration, as depicted in Figure 20.

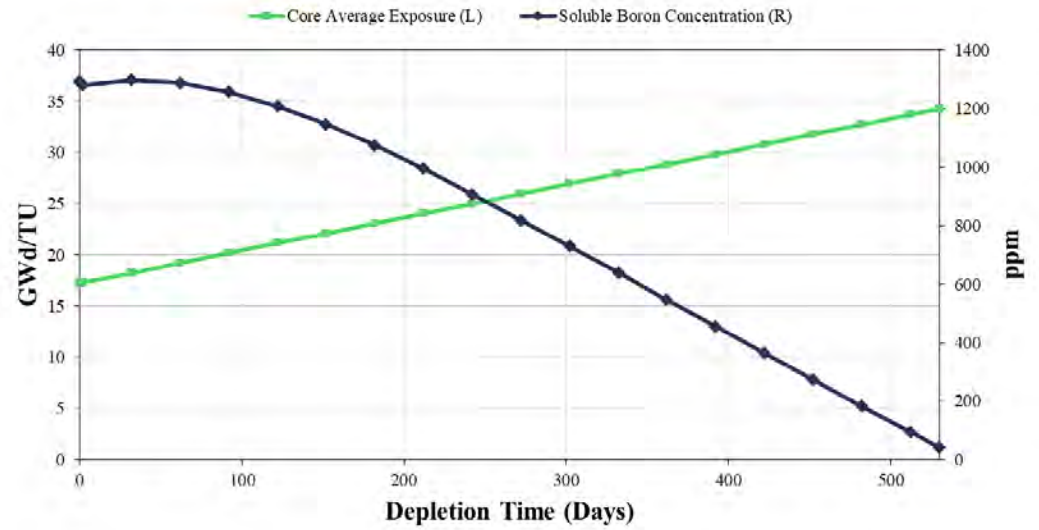

Figure 20. Equilibrium cycle core average exposure and soluble boron concentration vs. burnup.

The core design, shuffling scheme, and depletion cycle performance data from this equilibrium cycle were used to inform the reactor safety analysis performed in RELAP5-3D. This data included the case matrix cross section library developed in POLARIS and 3D maps of the relative power fraction and assembly-averaged burnup at 0 (BOC), 242 (MOC), and 530 (EOC) effective full power days. These values were used to improve the modelling and representation of the reactor core performance during the subsequent analyses in RELAP5-3D. APPENDIX B – EQUILIBRIUM CYCLE PERFORMANCE IN PARCS DETAIL shows the relative performance of the equilibrium cycle shuffling scheme.

3. RELAP5-3D SYSTEM MODELING FOR REACTOR SAFETY ANALYSIS

There are three major components to the reference PWR model developed in RELAP5-3D: first, hydrodynamic elements representing the coolant pipes and connections; second, the heat structures representing the fuel assemblies in the core; and third, a neutron diffusion module representing the fission power generation in the core. The hydrodynamic elements include pipes, branches, junctions, pumps, time-dependent volumes, etc. The heat structures were modeled to represent individual fuel assemblies in the core with a 1-to-1 connection. General description of RELAP5-3D and its capabilities is provided in APPENDIX A – NUCLEAR SYSTEM CODES .

The reference system to be simulated in this work is a typical four loop PWR power plant. All major flow paths for both primary and secondary systems are described, including the main steam and feed systems. Also modeled are primary and secondary power-operated relief valves and safety valves. The emergency core cooling system was included in the modeling of the primary side, and the auxiliary feedwater system was included in the secondary side modeling. A description of the primary and the secondary systems is presented in the following sections.

1. Reactor vessel – the reactor vessel model, as schematically shown in Figure 21, includes the downcomer, downcomer bypass, lower plenum, core, upper plenum, and upper head. The following leakage paths are represented in the vessel model: downcomer to upper plenum, cold leg inlet annulus to upper plenum, and upper plenum to the upper head by way of the guide tubes. Heat structures represent both external and internal metal mass of the vessel as well as the core rods. Decay heat was assumed to be at the American Nuclear Society-5.1 standard rate.

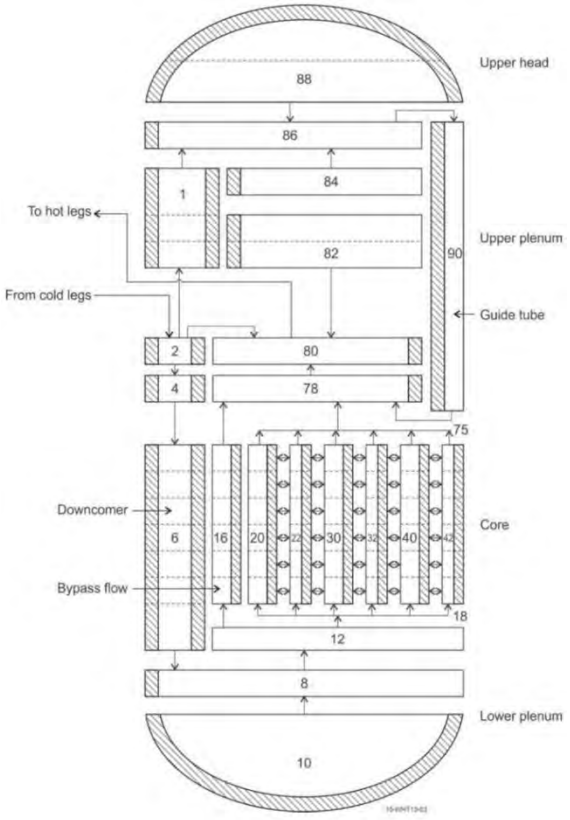

Figure 21. RELAP5-3D nodalization diagram for the reference PWR reactor vessel.

2. Reactor coolant system – The four primary coolant loops in the typical PWR model, as shown in Figure 22, are designated as loops A, B, C, and D. Each modeled loop contained a hot leg, U-tube steam generator, pump suction leg, pump, and cold leg. The pressurizer was attached to the C loop and the pressurizer spray lines were attached to the cold leg. Heat structures were added to each volume in the primary loops to represent the metal mass of the piping and steam generator tubes.

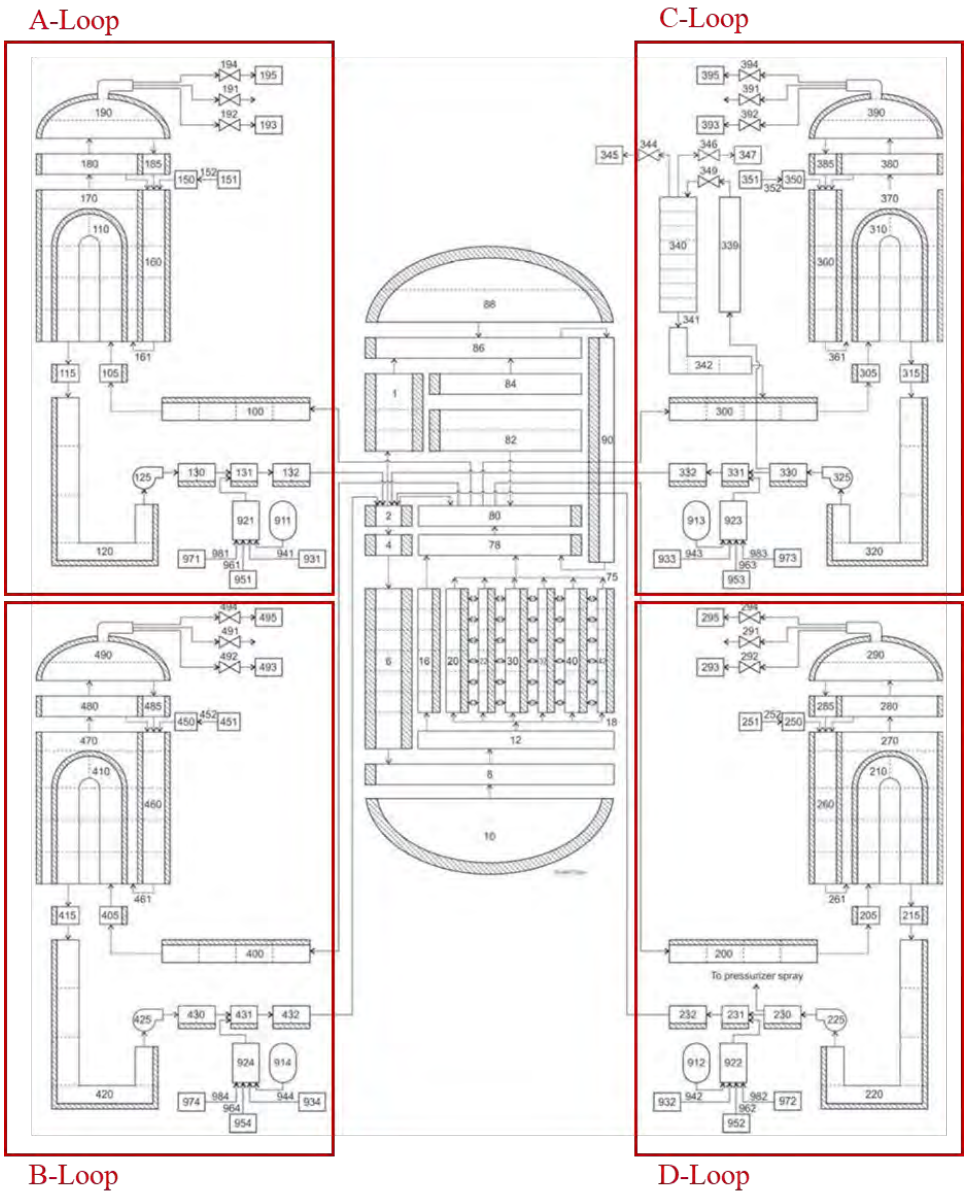

Figure 22. RELAP5-3D nodalization of a typical four-loop PWR primary system.

3. Balance of plant (partial) – the secondary system of the plant is also modeled. The steam generator secondary side model represents the major flow paths in the secondary system and includes the downcomer, boiler region, separator and dryer region, and the steam dome. The major flow paths of the steam line out to the turbine governor valves are modeled. Each line from the steam generator secondary out to the common steam header is modeled individually, and includes a main steam line isolation valve, a check valve, safety relief valves, and power-operated relief valves.

4. Feedwater system – the major flow paths of the feedwater system are modeled. The feedwater system consisted of the main feedwater system and the auxiliary feedwater system. The control system models include a steam dump control system, steam generator level control, pressurize pressure control system, and pressurizer level control systems, etc. Heat structures for the secondary system included the internal and external metal mass for each of the steam generators.
5. Emergency core cooling system – Attached to each cold leg is a low-pressure injection (LPI) connection port and an accumulator with its associated piping. A high-pressure injection (HPI) is also attached to each cold leg. The LPI and HPI models were set up to inject one-fourth of the total HPI and LPI flow into each loop. The RELAP5-3D model developed here can be used to perform simulations of various accident scenarios.

In addition, the reactor core data described in the previous section was adapted into the RELAP5-3D input deck. The 17×17 core assemblies were grouped into six concentric hydrodynamic elements (i.e., pipes) as shown in Figure 23, with an additional outermost hydrodynamic element for the reflector. The flow area of each pipe was a multiple of the flow areas of fuel assemblies within the pipe. Crossflow connections between the pipes were modeled using multiple junction elements.

	A	B	C	D	E	F	G	H	J	K	M	N	P	Q	R	S	T
1					7	7	7	7	7	7	7	7	7				
2			7	7	7	6	6	6	6	6	6	6	7	7	7		
3		7	7	6	6	6	5	5	5	5	5	6	6	6	7	7	
4		7	6	6	5	5	5	4	4	4	5	5	5	6	6	7	
5	7	7	6	5	5	4	4	4	3	4	4	4	5	5	6	7	7
6	7	6	6	5	4	4	3	3	3	3	3	4	4	5	6	6	7
7	7	6	5	5	4	3	3	2	2	2	3	3	4	5	5	6	7
8	7	6	5	4	4	3	2	2	1	2	2	3	4	4	5	6	7
9	7	6	5	4	3	3	2	1	1	1	2	3	3	4	5	6	7
10	7	6	5	4	4	3	2	2	1	2	2	3	4	4	5	6	7
11	7	6	5	5	4	3	3	2	2	2	3	3	4	5	5	6	7
12	7	6	6	5	4	4	3	3	3	3	3	4	4	5	6	6	7
13	7	7	6	5	5	4	4	4	3	4	4	4	5	5	6	7	7
14		7	6	6	5	5	5	4	4	4	5	5	5	6	6	7	
15		7	7	6	6	6	5	5	5	5	5	6	6	6	7	7	
16			7	7	7	6	6	6	6	6	6	6	7	7	7		
17					7	7	7	7	7	7	7	7	7				

Figure 23. The 17×17 core assemblies grouped into six concentric hydrodynamic elements (1 ~ 6) and one reflector element (7).

A total of 257 heat structure elements were modeled in the RELAP5-3D input deck, each having 19 axial nodes, totaling 4,883 nodes. The heat source of each node was linked to an individual hydrodynamic zone mapped in zone figures, defined in the nodal kinetics module. The zone figures are linked to composition figures, each of which is defined in the input deck using POLARIS cross section results. Note that POLARIS output is generated for select depletion points, both with control rods inserted

(rodded) and control rods out (un-rodded) scenarios. Linear interpolations were performed for nodes whose burnup data falls in between POLARIS depletion points, for both rodded and un-rodded scenarios. Figure 24 shows the histogram of burnup levels from 3281 fuel nodes, excluding reflector and blanket nodes, binned among the POLARIS select depletion points from 0 to 65 MWd/kgU. These burnup values include values gathered from the beginning, middle, and end of cycles.

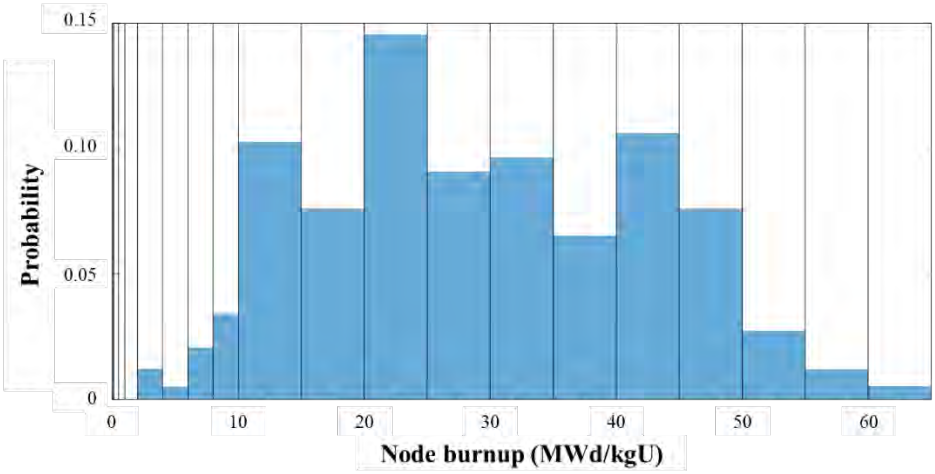

Figure 24. Histogram of node burnups binned among known data points from POLARIS depletion scenarios

In total, 133 hydrodynamic zones and 818 node compositions were defined in the input deck. A programming script was developed to automate the import of POLARIS data and to generate the RELAP5-3D input deck for the steady-state model. This script will be modified to generate transient input decks in the next fiscal year. As such, the safety analysis results will be presented in the next report in FY25.

4. SUMMARY AND FUTURE WORK

In FY24, research and development efforts were primarily focused on laying the groundwork for evaluating various significant power uprate strategies. The core and system models for reactor performance and safety analysis were developed based on the HE-LL-O core model of the reference PWR. These models incorporated design information collected in previous studies to ensure an accurate and robust analysis.

PARCS was employed to solve the time-dependent two-group neutron diffusion equation in three-dimensional Cartesian geometry. This tool enabled efficient and accurate calculations, ensuring that the study remained relevant to industry needs and could potentially accelerate the licensing process for the identified optimal design approach. To support these calculations, fuel assembly models for a 17×17 fuel lattice in POLARIS were developed, generating a multi-parametrized cross-section library. For validation purposes, a detailed reference PWR core model was developed using SERPENT2. The cycle depletion results using the PARCS model were verified against those generated using SERPENT2 to ensure that the deterministic models remained accurate. A near-optimal equilibrium cycle for the reference PWR core was also developed using a newly-created fuel shuffling scheme. This equilibrium cycle was designed to meet the energy production requirements, ensuring an 18-month cycle length while adhering to various operational and safety limits, including maximum discharge burnup, power peaking factors, and peak boron concentration.

In addition to core modeling, a reactor system model was developed using the RELAP5-3D simulation tool. This model was based on a typical four-loop PWR with a core power output of 3,850 MWt. The core adopted nodal kinetics calculations, leveraging the NESTLE module. Neutron yields and cross-section data generated by the POLARIS tool were transferred to this nodal kinetics module to support the simulations. Initially, a steady-state model was developed, with plans to expand this into transient models in the upcoming fiscal year. These transient analyses will help determine whether safe operational parameters are met under accident scenarios, providing valuable insights into the feasibility of significant power uprates.

5. REFERENCES

[1] Nuclar Regulatory Comission, "Power Uprates for Nuclear Plants," Nuclar Regulatory Comission, January 2022. [Online]. Available: https://www.nrc.gov/reading-rm/doc-collections/fact-sheets/power-uprates.html. [Accessed 1 August 2024].

[2] R. Szilard, H. Zhang, A. Epiney, C. Parisi and P. Talbot, "Loss of Coolant Accident / Emergency Core Coolant System Evaluation of Risk-Informed Margins Management Strategies for a Representative Pressurized Water Reactor (INL/EXT-16-39805)," Idaho National Laboratory, Idaho Falls, ID, USA, 2016.

[3] T. Downar, Y. Xu and V. Seker, "PARCS v3.0 U.S. NRC Core Neutronics Simulator User Manuel (UM-NERS-09-0001)," University of Michigan , Ann Arbor, MI, USA, 2010.

[4] J. Leppanen, M. Pusa, T. Viitanen, V. Valtavirta and T. Kaltiaisenaho, "The Serpent Monte Carlo code: Status, development and applications in 2013," *Annals of Nuclear Energy*, vol. 82, pp. 142-150, 2015.

[5] M. A. Jessee, W. A. Wieselquist, T. M. Evans, S. P. Hamilton, J. J. Jarrell, K. S. Kim, J. P. Lefebvre, R. A. Lefebvre, U. Mertyurek, A. B. Thompson and M. L. Williams, "POLARIS: A new two-dimensional lattice physics analysis capability for the SCALE code system," in *PHYSOR 2014 - The Role of Reactor Physics toward a Sustainable Future*, Kyoto, Japan, 2014.

[6] A. S. Epiney, A. Alfonsi, C. Parisi and R. Szilard, "RISMC industry application #1 (ECCS/LOCA): Core characterization automation: Lattice codes interface for PHISICS/RELAP5-3D," *Nuclear Engineering and Design*, vol. 345, pp. 15-27, 2019.

[7] The RELAP5-3D Code Development Team, "RELAP5-3D Code Manual Volume 1: Code Structure, System Models and Solution Methods," Idaho National Laboratory, Idaho Falls, ID, USA, 2005.

[8] P. Turinsky, R. M. Al-Chalabi, P. Engrand, H. N. Sarsour, F. X. Faure and W. Guo, "NESTLE: Few-group neutron diffusion equation solver utilizing the nodal expansion method for eigenvalue, adjoint, fixed-source steady-state and transient problems," Los Alamos National Laboratory, Los Alamos, NM, USA., 1994.

ACKNOWLEDGEMENTS

This research made use of Idaho National Laboratory's High Performance Computing systems located at the Collaborative Computing Center and supported by the Office of Nuclear Energy of the U.S. Department of Energy and the Nuclear Science User Facilities under Contract No. DE-AC07-05ID14517.

Page intentionally left blank

APPENDIX A – NUCLEAR SYSTEM CODES

SCALE/POLARIS

POLARIS 2D lattice physics capability in the SCALE code system for LWR analysis. It uses a 2D method of characteristics (MOC) neutron transport solver, and the Embedded Self Shielding Method (ESSM) for multigroup cross section processing.

PARCS

A 3D reactor core simulator which solves steady-state and time-dependent multigroup diffusion equations. The multigroup diffusion constants need to be provided. These are generally generated by a lattice code.

GENPMAXS

Generates cross section libraries readable for PARCS from formats .t16

SERPENT

A 3D continuous-energy neutron and photon transport code, developed at VTT. The standard geometry model relies on a universe-based constructive solid geometry type. Neutron interaction physics in SERPENT2 is based on classical collision kinematics and ENDF reaction laws. Cross sections are read from ACE format data libraries. The format was originally developed for the MCNP code from Los Alamos National Laboratory, and is also used by other Monte Carlo codes, such as OpenMC and Geant4. The continuous-energy interaction data is produced from evaluated nuclear data files without major approximations.

SERPENT2 features built-in burnup calculation capability for tracking the nuclide concentrations subject to neutron interactions and radioactive decay. The methodology is applicable to nuclear fuel and activated materials. Depletion zone division and the formation of transmutation and decay paths is accomplished automatically, with minimal input from the user. SERPENT2 uses the Chebyshev Rational Approximation method for the solution of the Bateman depletion equations and provides various time integration methods to perform the iterations between the neutronics and depletion solution.

RELAP5-3D

The RELAP5-3D [7] code has been developed for best-estimate transient simulation of LWR coolant systems during postulated accidents. Specific applications of the code have included simulations of transients in LWR systems such as loss of coolant, anticipated transients without scram, and operational transients such as loss of feedwater, loss of offsite power, station blackout, and turbine trip. RELAP5-3D, the latest in the series of RELAP5 codes, is a highly generic code that, in addition to calculating the behavior of a reactor coolant system during a transient, can be used for simulation of a wide variety of hydraulic and thermal transients in both nuclear and nonnuclear systems involving mixtures of vapor, liquid, non-condensable gases, and nonvolatile solute.

RELAP5-3D is suitable for the analysis of all transients and postulated accidents in LWR systems, including both large- and small-break loss-of-coolant accidents as well as the full range of operational and fusion reactor transient applications. Additional capabilities include space reactor simulations, gas cooled reactor applications, fast breeder reactor modeling, and cardiovascular blood flow simulations.

The RELAP5-3D code is based on a non-homogeneous and non-equilibrium model for the two-phase system that is solved by a fast, partially implicit numerical scheme to permit economical calculation of system transients. The objective of the RELAP5-3D development effort from the outset was to produce a code that included important first-order effects necessary for accurate prediction of system transients but that was sufficiently simple and cost effective so that parametric or sensitivity studies were possible.

The code includes many generic component models from which general systems can be simulated. The component models include pumps, valves, pipes, heat releasing or absorbing structures, reactor kinetics, electric heaters, jet pumps, turbines, compressors, separators, annuli, pressurizers, feedwater heaters, Emergency Core Cooling (ECC) mixers, accumulators, and control system components. In addition, special process models are included for effects such as form loss, flow at an abrupt area change, branching, choked flow, boron tracking, and non-condensable gas transport.

The system mathematical models are coupled into an efficient code structure. The code includes extensive input checking capability to help the user discover input errors and inconsistencies. Also included are free-format input, restart, renodalization, and variable output edit features. These user conveniences were developed in recognition that generally the major cost associated with the use of a system transient code is in the engineering labor and time involved in accumulating system data and developing system models, while the computer cost associated with generation of the final result is usually small.

A specific model that is important for this report's analysis is the NESTLE nodal kinetic code [8]. It is a code system that can solve the few-group neutron diffusion equation using the nodal expansion method (NEM) for eigenvalue criticality, eigen value adjoint, external fixed-source steady-state, and external fixed-source or eigenvalue initiated transient problems. The NEM utilizes a nonlinear iterative strategy which allows it to solve either the nodal or finite difference method (FDM) representation of the few-group neutron diffusion equation. The eigenvalue problem completes criticality searches and the external fixed-source steady-state problem searches to achieve a prescribed power level.

APPENDIX B – EQUILIBRIUM CYCLE PERFORMANCE IN PARCS

The following figures detail the relative performance of the equilibrium cycle shuffling scheme, showing the distribution of the assembly-averaged radial relative power fraction, the assembly-averaged radial exposure, the node-averaged axial relative power fraction, and the node-averaged axial relative power fraction at both the beginning (BOC) and end (EOC) of the equilibrium cycle.

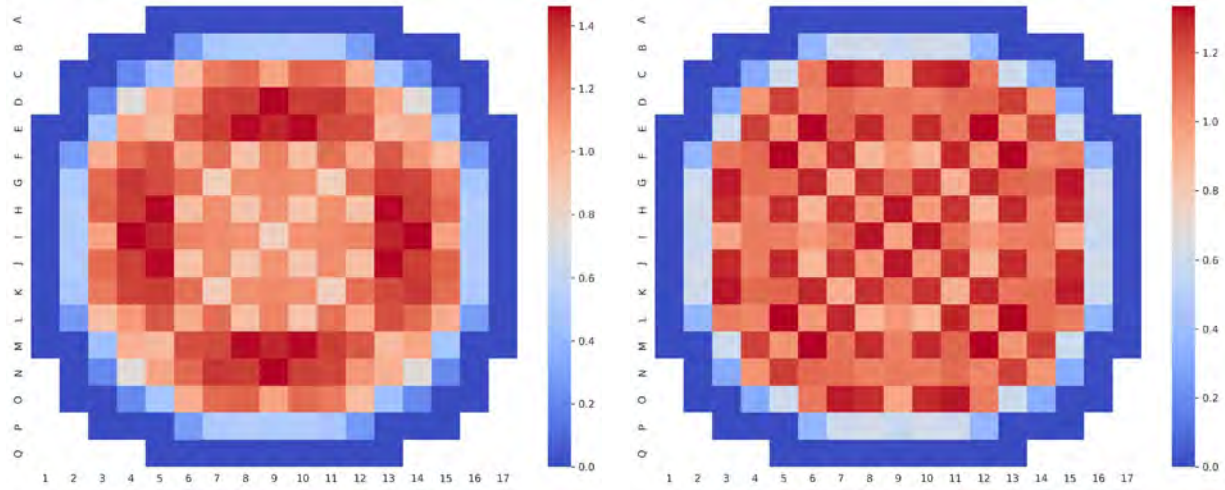

(a) (b)

Figure 25. Assembly-averaged radial relative power fraction. (a) BOC, and (b) EOC.

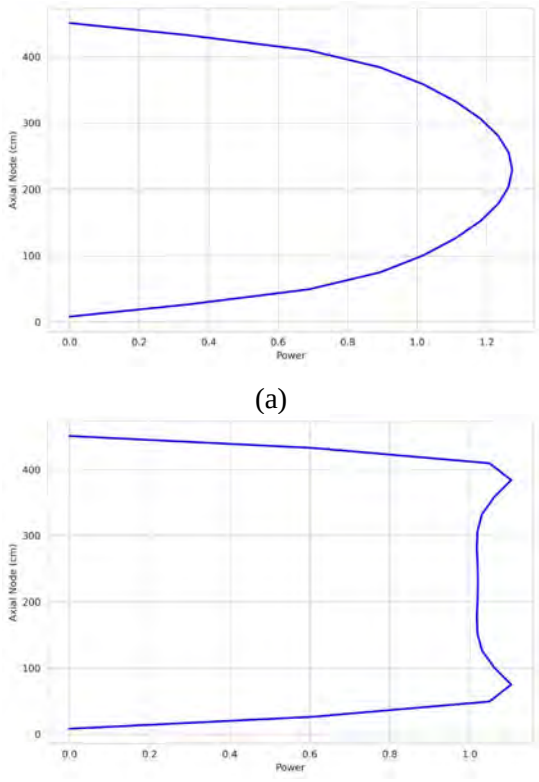

(a)

(b)

Figure 26. Node-averaged axial relative power fraction. (a) BOC, and (b) EOC.

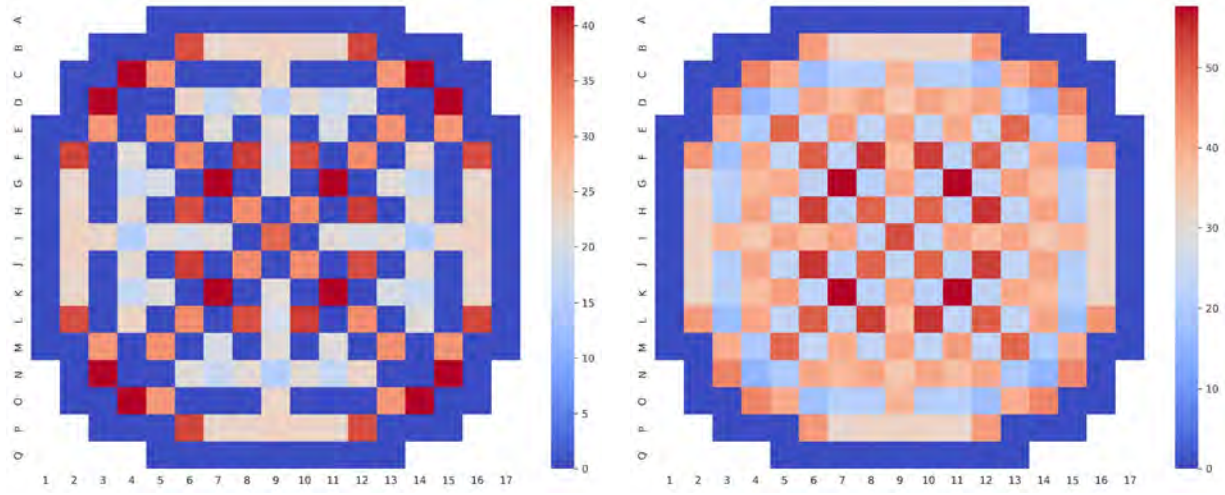

(a) (b)

Figure 27. Assembly-averaged radial exposure. (a) BOC, and (b) EOC.

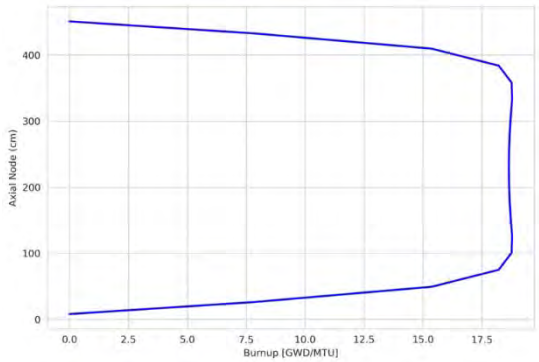

(a)

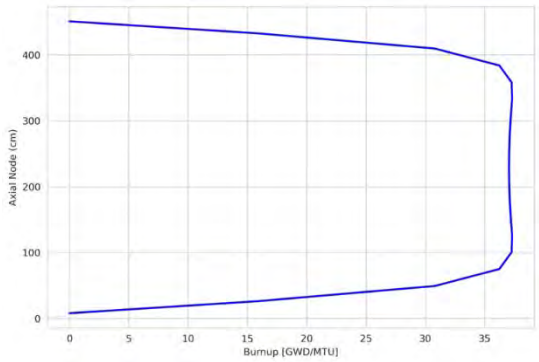

(b)

Figure 28. Node-averaged axial exposure. (a) BOC, and (b) EOC.